

ACTIVE GALACTIC NUCLEUS ENVIRONMENTS AND FEEDBACK TO NEIGHBORING GALAXIES AT
 $Z \sim 5$ PROBED BY LYMAN-ALPHA EMITTERS*

SATOSHI KIKUTA,^{1,2} MASATOSHI IMANISHI,^{1,2} YOSHIKI MATSUOKA,^{1,2,3} YUICHI MATSUDA,^{1,2} KAZUHIRO SHIMASAKU,^{4,5} AND
FUMIAKI NAKATA⁶

¹*Department of Astronomical Science, SOKENDAI (The Graduate University for Advanced Studies),
Osawa, Mitaka, Tokyo 181-8588, Japan*

²*National Astronomical Observatory of Japan, Osawa, Mitaka, Tokyo 181-8588, Japan*

³*Research Center for Space and Cosmic Evolution, Ehime University, Matsuyama, Ehime 790-8577, Japan.*

⁴*Department of Astronomy, Graduate School of Science, The University of Tokyo, Tokyo 113-0033, Japan*

⁵*Research Center for the Early Universe, The Graduate School of Science, The University of Tokyo, Tokyo 113-0033, Japan*

⁶*Subaru Telescope, 650 North Aohoku Place, Hilo, HI 96720, USA*

(Received; Revised; Accepted)

Submitted to ApJ

ABSTRACT

Active galactic nuclei (AGNs) in the high-redshift Universe are thought to reside in overdense environments. However, recent works provide controversial results partly due to the use of different techniques and possible suppression of nearby galaxy formation by AGN feedback. We conducted deep and wide-field imaging observations with the Suprime-Cam on the Subaru telescope and searched for Lyman-alpha emitters (LAEs) around two QSOs (quasi-stellar objects) at $z \sim 4.9$ and a radio galaxy at $z \sim 4.5$ by using narrow-band filters to address these issues more robustly. In the QSO fields, we obtained additional broad-band images to select Lyman-break galaxies (LBGs) at $z \sim 5$ for comparison. We constructed a photometric sample of 301 LAEs and 170 LBGs in total. A wide field of view ($34' \times 27'$, corresponding to 80×60 comoving Mpc²) of the Suprime-Cam enabled us to probe galaxies in the immediate vicinities of the AGNs and in the blank fields simultaneously and compare various properties of them in a consistent manner. The two QSOs are located near local density peaks ($< 2\sigma$) and one of the QSOs has a close companion LAE with projected separation of 80 physical kpc. The radio galaxy is found to be near a void of LAEs. The number densities of LAEs/LBGs in a larger spatial scale around the AGNs are not significantly different from those in blank fields. No sign of feedback is found down to $L_{\text{Ly}\alpha} \sim 10^{41.8}$ erg s⁻¹. Our results suggest that high-redshift AGNs are not associated with extreme galaxy overdensity and that this cannot be attributed to the effect of AGN feedback.

Keywords: galaxies: formation — galaxies: high-redshift — quasars: general — quasars: individual
(SDSS J080715.2+132805, SDSS J111358.3+025333, 4C 04.11)

satoshi.kikuta@nao.ac.jp

Corresponding author: Satoshi Kikuta

* Based on data collected at Subaru Telescope, which is operated by the National Astronomical Observatory of Japan.

1. INTRODUCTION

Supermassive black holes (SMBHs) at the center of galaxies provide us various insights into key physics of galaxy formation and evolution. The correlation between the properties of SMBHs and those of the host galaxies such as masses and velocity dispersions of spheroidal components (Magorrian et al. 1998; Ferrarese & Merritt 2000) indicates that active galactic nuclei (AGNs; rapidly growing SMBHs) and star formation activities are physically connected and that AGNs play a crucial role in galaxy formation. However, details of their formation and growth history still remain largely unknown. To date, SMBHs with BH masses in excess of $10^9 M_\odot$ are known to already exist at the very beginning of the Universe ($z > 6$; e.g., Mortlock et al. 2011; Wu et al. 2015). Where and how these SMBHs are formed and evolved in pace with their host galaxies is a fundamental question to elucidate galaxy evolution.

It is expected that high-redshift SMBHs should reside more frequently in highly biased regions of the Universe where the dark matter and galaxies are overly clustered (e.g., Volonteri & Rees 2006). Locating such overdense regions at high-redshift Universe, the so-called ‘‘protoclusters’’ (Shimasaku et al. 2003; Matsuda et al. 2010; Toshikawa et al. 2012, see Overzier 2016 for a recent review) has a potential to provide us opportunities to probe how environmental differences in galaxy evolution observed at the local Universe (Dressler 1980; Cappellari et al. 2011) are established. Since searching for protoclusters without signposts like AGNs is difficult because of their rarity, probing AGN environments gives us clues to environmental effects on galaxy evolution as well as growth history of SMBHs.

Environments of high-redshift quasi-stellar objects (QSOs; luminous type 1 AGNs) and radio galaxies (RGs, radio-loud type 2 AGNs) have been extensively studied with the motivation described above. Radio-loud AGNs (RGs and radio-loud QSOs) are typically found in overdense regions using various methods to locate galaxies around them, including the Lyman break technique, narrow-band imaging, and Spitzer/Infrared Array Camera (IRAC) color-selection (Zheng et al. 2006; Venemans et al. 2007; Matsuda et al. 2009; Wylezalek et al. 2013). On the other hand, the situation is different for (radio-quiet) QSOs. While measurements of QSO clustering shows that they should reside in massive dark matter halos ($M_h > 10^{12} M_\odot$) up to $z < 4$ (Shen et al. 2007; Trainor & Steidel 2012; Garcia-Vergara et al. 2017, see also Eftekharzadeh et al. 2015), many authors found both galaxy overdensity associated with QSOs (Utsumi et al. 2010; Capak et al. 2011; Falder et al.

2011; Swinbank et al. 2012; Husband et al. 2013; Morselli et al. 2014) and normal or underdensity around QSOs (Francis & Bland-Hawthorn 2004; Kashikawa et al. 2007; Kim et al. 2009; Bañados et al. 2013; Simpson et al. 2014; Adams et al. 2015; Mazzucchelli et al. 2017), again using various technique to identify galaxies in the QSO fields. Even in fields around intermediate-redshift QSO multiples, their environments are not always rich (Boris et al. 2007; Farina et al. 2013; Sandrinelli et al. 2014), though Hennawi et al. (2015) found an overdensity around a quasar quartet.

Several authors suggest that strong UV radiation from AGNs can suppress the formation of low-mass galaxies around them by heating and photoevaporating their gas (Kashikawa et al. 2007; Utsumi et al. 2010; Bruns et al. 2012), and thereby dilute any sign of overdensity and mitigate the discrepancy observed to date. The deficit of H I gas with column density $N_H < 10^{17} \text{ cm}^{-2}$ (Lyman-alpha forest) within a few to several physical Mpc (pMpc) from QSOs has been well known as the QSO proximity effect (Bechtold 1994; Calverley et al. 2011). However, it is unclear whether this QSO’s radiative feedback is indeed strong enough to suppress the formation of neighboring low-mass galaxies ($N_H > 10^{20} \text{ cm}^{-2}$). On the other hand, Cantalupo et al. (2012) claimed that fluorescently illuminated gas around a hyperluminous QSO can boost Ly α luminosity of galaxies around the QSO.

Mixed results about QSO environments obtained so far can be partly due to the use of different observational techniques, survey depths, and field coverages, as well as various feedback effects. Many studies used the Lyman break technique to identify high-redshift galaxies around QSOs. However, this technique sample galaxies from wide redshift range of, say, $\Delta z \sim 1$ (Yoshida et al. 2006). At $z \sim 5$, this corresponds to ~ 100 pMpc. This scale is far larger than the expected size of the largest protocluster and known QSO proximity, hence galaxies selected by this method contain many foreground and background, physically unrelated galaxies. Moreover, even if AGNs have associated structures of a scale of a few to several pMpc, or if AGNs affect surrounding galaxies within this scale, it should be smeared out by the projection effect. If one wants to study AGN environments and feedback to their neighbors, it is particularly important to pick up galaxies within the AGN’s proximity in both tangential and radial (redshift) directions.

Wide-field, narrow-band imaging observations are currently the best way to securely investigate AGN environments and feedback unless a large spectroscopic sample is available. Narrow-band filters have full widths at half maximum (FWHMs) of $\lesssim 100\text{\AA}$ and they enable us

to select line emitting galaxies from a narrow redshift range of $\Delta z \lesssim 0.1$. In particular, galaxies whose redshifted Ly α emission fall inside a narrow-band filter, the so-called Lyman-alpha emitters (LAEs), are commonly found at $z > 2$. At $z \sim 5$, $\Delta z \sim 0.1$ corresponds to ~ 10 pMpc. This scale is sufficiently small to detect proto-clusters of this redshift (Chiang et al. 2013) and matches measured QSO's proximity sizes (Calverley et al. 2011). With narrow-band filters, we can select LAEs within the AGNs proximity in radial (redshift) direction, by minimizing the contamination from physically unrelated foreground and background galaxies. Furthermore, majority of LAEs are known to have low stellar mass (Gawiser et al. 2006; Finkelstein et al. 2007; Ono et al. 2010a,b) and therefore more susceptible to AGN feedback than massive galaxies. Thus, LAEs are best suited to observationally scrutinize whether and how the properties of low-mass galaxies around AGNs are altered compared to general fields, by overcoming the uncertainties in previous works.

In this paper, we present the results of our deep and wide-field observations around two QSOs at $z \sim 4.9$ and one RG at $z \sim 4.5$ using the Suprime-Cam (S-Cam, Miyazaki et al. 2002) on the Subaru telescope. Narrow-band filters well covering the proximity of these AGNs in the radial direction and the wide field of view (FoV) of S-Cam ($34' \times 27'$, or 13×10 pMpc at $z = 5$) enables us to detect galaxies within and outside of the AGN's proximity simultaneously, as opposed to previous narrow-band studies with smaller FoVs (Swinbank et al. 2012; Bañados et al. 2013; Mazzucchelli et al. 2017). We try to identify the effect of AGN feedback by comparing the luminosity functions (LFs) within and outside of the AGN proximity, because radiative feedback affects galaxies differently depending on their mass.

The structure of this paper is as follows: in Section 2, we describe our imaging observations and data reduction. In Section 3 we present our photometric selection of LAEs and LBGs and subsequent analyses. We show our main results and discuss them in Section 4 and present the summary and conclusion in Section 5. Throughout this paper, we use the AB magnitude system and adopt a Λ CDM cosmology, with $H_0 = 71 \text{ km s}^{-1} \text{ Mpc}^{-1}$, $\Omega_M = 0.27$, $\Omega_\Lambda = 0.73$ (Komatsu et al. 2009).

2. OBSERVATIONS AND DATA REDUCTION

We conducted imaging observations of two fields around QSOs at $z \sim 4.9$, SDSS J080715.2+132805 (08^h07^m15^s.1, +13°28'05".2, $z = 4.885$, Trakhtenbrot et al. 2011, hereafter J08 field) and SDSS J111358.3+025333 (11^h13^m58^s.3 +02°53'33".7, $z = 4.870$, Trakhtenbrot et al.

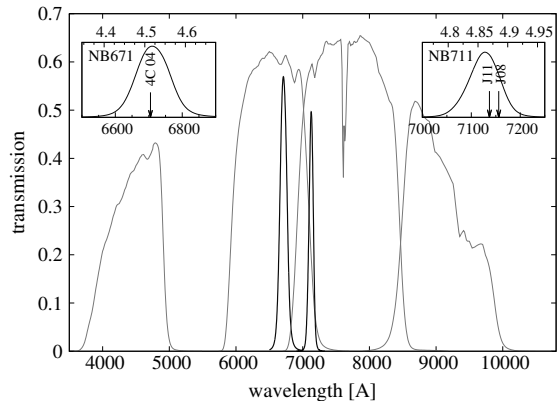


Figure 1. Transmission curves of filters we used. Thin curves indicate transmission of broad-band filters (from left to right, B , R , i' , and z'). Thick curves on the left (right) shows that of $NB711$ ($NB671$). Insets show enlarged transmission curves of narrow-band filters. The upper axis shows corresponding Ly α redshift. The redshift of AGNs are marked with arrows.

2011, hereafter J11 field) using the Suprime-Cam (Miyazaki et al. 2002) on the 8.2m Subaru Telescope in 2014 Dec 21–26 and 2015 Dec 16–17 (UT; Program ID: S14B-006 and S15B-010, PI: M. Imanishi). As we illustrate in Figure 1, we used broad-band filters (R , i' , and z') and a narrowband filter $NB711$ ($\lambda_c = 7126 \text{ \AA}$, $\Delta\lambda = 73 \text{ \AA}$) to sample LAEs in the redshift range of $4.83 \lesssim z \lesssim 4.89$ and LBGs at $z \sim 5$. The redshifts of J08 and J11 are measured to be within this range in Trakhtenbrot et al. (2011) using the Mg II emission line, which is known to be good redshift indicator of type 1 AGNs (Hewett & Wild 2010; Shen et al. 2016). Note that, because their redshifts fall in the redder part of the sensitivity of $NB711$ and LAEs are more easily selected in bluer side of the $NB711$ bandpass, there is a possibility that we detect LAEs at slightly different redshift. If true systemic redshifts of the AGNs are larger than the observed values, our measurements are affected further. The median and intrinsic scatter of Mg II redshift with respect to the narrow [O II] line is measured to be -62 km s^{-1} and 220 km s^{-1} , respectively¹ (Shen et al. 2016). Assuming Gaussian distribution, the probability of J08 having redshift higher than 4.89 is thus $\lesssim 6\%$. M_{BH} of these two QSOs are also derived from the Mg II line and found to be very massive at $z \sim 5$. Specifically, they have SMBHs with mass of $10^{9.24} M_\odot$ for J08 and $10^{9.12} M_\odot$ for J11.

¹ Also note that, in Trakhtenbrot et al. (2017), they detected [C II] emission line in six AGNs in the Trakhtenbrot et al. (2011) sample with ALMA and found velocity shifts of $\sim 500 \text{ km s}^{-1}$ between the Mg II line and the [C II] line.

Table 1. Information about our targets and observations.

Object name	Redshift ^a	$\log M_{\text{BH}}^{\text{a}}$ (M_{\odot})	$\log L_{\text{bol}}^{\text{a}}$ (erg s^{-1})	Exposure time (sec) and seeing ^b				
				B	R	i'	z'	NB^{c}
SDSS J080715.2+132805	4.885	9.24	47.07	...	6000	4500	4200	9000
				...	1.1''	1.0''	1.3''	0.9''
SDSS J111358.3+025333	4.870	9.12	46.89	...	3300	3900	3000	11700
				...	0.9''	0.9''	1.0''	0.8''
4C 04.11	4.514	$\gtrsim 9$...	4500	3600	5400	...	24000
(03 ^h 11 ^m 48 ^s .0, +05°08'01''5)				0.9''	0.8''	0.9''	...	0.9''

^aFrom Trakhtenbrot et al. (2011) (J08 and J11) and Parijskij et al. (2014) (4C04).

^bExposures during poor conditions were discarded.

^c $NB711$ for J08 and J11 fields and $NB671$ for 4C04 field.

Additionally, we obtained S-Cam broad-band (B , R , and i') and narrow-band ($NB671$, $\lambda_c = 6712 \text{ \AA}$, $\Delta\lambda = 120 \text{ \AA}$) images of an RG at $z = 4.514$ from the data archive (Program ID: S09B-070N, PI: Y. Matsuda). We can detect LAEs at $z = 4.47\text{--}4.57$ with $NB671$. This RG, namely 4C 04.11 (also known as RC J0311+0507; 03^h11^m48^s.0, +05°08'01''5 at $z = 4.514$, hereafter 4C04 field) has an estimated luminosity at rest-frame 500 MHz of $3 \times 10^{29} \text{ W Hz}^{-1}$, or luminosity at rest-frame 2.7 GHz of $L_{2.7\text{GHz}} = 6 \times 10^{34} \text{ erg s}^{-1} \text{ Hz}^{-1} \text{ sr}^{-1}$. For reference, the sample in Venemans et al. 2007 has at most radio luminosity of $L_{2.7\text{GHz}} = 2.0 \times 10^{34} \text{ erg s}^{-1} \text{ Hz}^{-1} \text{ sr}^{-1}$. Its very high radio luminosity and a highly asymmetric Fanaroff-Riley type II (FR II) structure jet suggest that it is powered by a SMBH of mass $\sim 10^9 M_{\odot}$ (Kopylov et al. 2006). The redshift of the RG is confirmed by various emission lines, such as the Ly α , [O II], and [Ne III] lines (Nesvadba et al. 2016) and well constrained within $z = 4.504\text{--}4.514$ (see the inset of Figure 1).

At $z \sim 5$, we can construct sufficiently large sample of galaxies with reasonable integration time. For J08 and J11 fields, the individual integration times in R , i' , z' , and $NB711$ were 300 sec, 300 sec, 300 sec, and 900 sec per pointing, respectively. For 4C04 fields, the individual integration times in B , R , i' , and $NB671$ were 450 sec, 450 sec, 360 sec, and 1200 sec per pointing, respectively. Each exposure was dithered by $\gtrsim 60''$. A N point circular dithering pattern ($N = 6, 9$) was used. Details of our targets and observations are listed in Table 1.

The raw data were reduced in a standard manner with the dedicated software package, SDFRED2 (Ouchi et al.

2004), which includes bias subtraction, flat-fielding, distortion correction, sky subtraction, image alignments, and stacking. The $NB711$ -band images were processed with L. A. Cosmic algorithm (van Dokkum 2001) to remove cosmic rays after the flat-fielding process. The world coordinate system of images were calibrated by comparing the USNO-B1.0 catalog. Mean offset from the catalog is $\sim 0.2''$. After we matched seeing of the images of each field to the worst one (see Section 3.1 and 3.2), we perform object detection and photometry using the double-image mode of SExtractor version 2.1.6 (Bertin & Arnouts 1996). We used the narrow-bands and the z' -band as detection bands for LAEs and LBGs, respectively. Spikes and halos around bright stars and low-S/N regions near the edge of FoV are masked during object detection. Objects in the masked regions or with SExtractor flags of > 2 are eliminated from our catalogs. SExtractor flag 1 means an object has close neighbor or bad pixels which affect photometry. SExtractor flag 2 means an object was originally blended with another one. We first include these sources and later visually check and eliminate obvious spurious and heavily blended ones to maximize the detection rate.

We use magnitudes and colors measured in 1.7 times PSF FWHM diameter apertures unless otherwise stated. Photometric calibration for the J08 and J11 fields was obtained from the spectrophotometric standard stars, GD 108 (Oke 1990) and GD 153 (Moehler et al. 2014), observed during the same night of the observations. Photometric calibration for the 4C04 field was obtained from SDSS stars in the field. We corrected the measured magnitudes for Galactic extinction of $E(B - V) = 0.03 \text{ mag}$ (J08), 0.04 mag (J11), and 0.19 mag (4C04)

(Schlegel et al. 1998). We note that the stellar colors measured in the J08 field are offset by ~ 0.1 – 0.2 mag from the Gunn & Stryker (1983) stellar templates on R - $NB711$ vs. $NB711$ - i' and R - i' vs. i' - z' color-color diagrams. Since the R - and i' -band magnitudes of stellar sources in the field are confirmed to be well matched with those of SDSS sources, we manually corrected the zero-points of $NB711$ - and z' -band. The reason for this offset is unclear, but may partly be due to the unstable weather condition of our observations. Finally, the locus of stellar sources on a color-color diagram in all the fields became consistent with those of Gunn & Stryker (1983) within $\simeq 0.05$ mag. Limiting magnitudes of our observations are given in Section 3.1 and Section 3.2.

3. ANALYSES

3.1. Selection of Lyman-alpha emitters

As image quality of our z' -band image is not as good as we expected because of weather conditions and z' -band magnitude is not required for LAE selection below, we matched seeing of images of J08 and J11 field to that of R -band (the worst one except for z' -band; see Table 1) when we construct LAE sample. The 3σ limiting magnitudes after all corrections in (R , i' , $NB711$) are (27.5, 27.1, 26.6) and (27.5, 27.3, 26.7) for J08 and J11 field, respectively. We chose LAEs at $z \sim 4.9$ from our catalog using the criteria below (Ouchi et al. 2003):

$$Ri_1 - NB711 > \max(0.8, 3\sigma(Ri_1 - NB711)) \quad (1)$$

$$R - i' > 0.5 \quad (2)$$

$$i' - NB711 > 0 \quad (3)$$

$$NB711 < 5\sigma_{NB711}, i' < 2\sigma_{i'}, \quad (4)$$

where $Ri_1 \equiv 0.5 \times R + 0.5 \times i'$ and $\sigma(Ri_1 - NB711)$ denotes the expected deviation of the quantity $Ri_1 - NB711$ for a flat continuum source. For objects fainter than 2σ in R -band, we replace the R -band magnitude by its 2σ limiting magnitude as a lower limit. Ouchi et al. (2003) showed that these criteria effectively remove contaminants such as low-redshift emitters and objects with a trough feature blueward of the $NB711$ -band filter. Shimasaku et al. (2003) conducted follow-up spectroscopy of five candidates selected by this criteria and found a contamination rate of about $\sim 20\%$, which is sufficiently low for our purpose.

In 4C04 field, 3σ limiting magnitudes in (B , R , i' , $NB671$) are (27.0, 26.8, 26.5, 26.5). We chose LAEs at $z \sim 4.5$ using the criteria below:

$$Ri_2 - NB671 > \max(0.5, 3\sigma(Ri_2 - NB671)) \quad (5)$$

$$i' - NB671 > 0 \quad (6)$$

$$NB671 < 5\sigma_{NB671}, i' < 2\sigma_{i'}, B > 3\sigma_B, \quad (7)$$

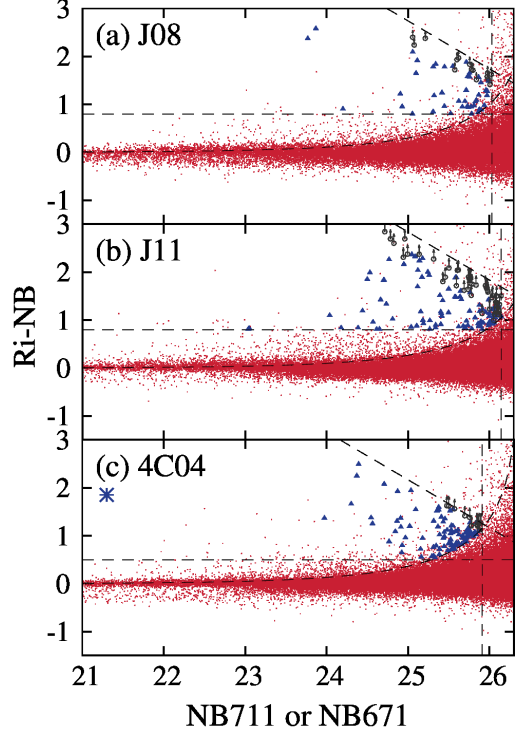


Figure 2. Distribution of sources in color-magnitude diagrams in (a) J08, (b) J11, and (c) 4C04 field. Red points show all sources in our catalog and blue triangles and gray circles with arrows show LAEs with and without R -band detection (2σ). The asterisk in panel (c) shows the location of the RG 4C 04.11, which is also selected as LAE. The QSO J08 and J11 are also selected as LAE but they have $NB711 < 21$. x -axis shows magnitude in $NB711$ -band in panel (a) and (b), $NB671$ in panel (c) and y -axis shows $Ri_1 - NB711$ in (a) and (b), and $Ri_2 - NB671$ in (c). The dashed lines denote the criteria used to select LAEs (see Section 3.1).

where $Ri_2 \equiv 0.8 \times R + 0.2 \times i'$ and $\sigma(Ri_2 - NB671)$ denotes the expected deviation of the quantity $Ri_2 - NB671$ for a flat continuum source. Similar criteria were used in Large-Area Lyman Alpha (LALA) survey (e.g. Rhoads et al. 2000) to detect LAEs at $z \sim 4.5$ and the success rate based on their spectroscopic follow-up campaign is about $\sim 70\%$ (Dawson et al. 2007; Zheng et al. 2013). In Figure 2 we show color-magnitude diagrams in each field.

Finally, we visually checked the images and eliminated some spurious sources such as ones clearly blending with other sources and ones on stellar halos or saturation spikes. Finally, we find 60, 136, and 105 LAEs in J08, J11, and 4C04 field, respectively. Then we divide LAEs into two subgroups: one is “proximity” sample, which is located within 3 pMpc (J08 and J11 fields) or 5 pMpc (4C04 field) from the central AGNs, the other is “blank fields” sample, which is the rest of the sample. The

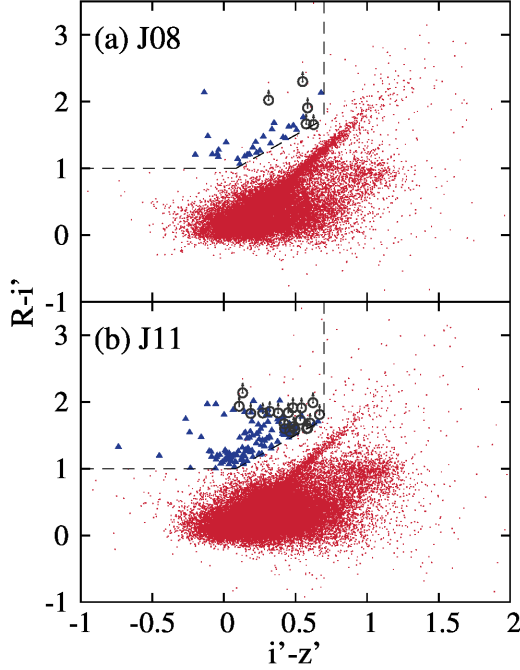


Figure 3. Distribution of sources in color-color diagrams in (a) J08 and (b) J11 field. Red points indicate all sources with 5σ detection in z' -band in our catalog, blue triangles and gray circles with arrows indicate LBGs with and without R -band detection (2σ). The dashed lines denote the criteria used to select LBGs (see Section 3.2).

size of the “proximity” of 3 or 5 pMpc is set by the FWHM of employed narrow-band filters ($\Delta\lambda_{\text{NB711}} = 72 \text{ \AA}$, $\Delta\lambda_{\text{NB671}} = 120 \text{ \AA}$), and these values are sufficiently small to detect overdensities or galaxies affected by AGN feedback at $z \sim 5$ (Chiang et al. 2013; Calverley et al. 2011). The sample size of proximity LAEs in J08, J11, and 4C04 field is respectively 14, 34, and 32.

3.2. Selection of Lyman-break galaxies at $z \sim 5$

When we matched seeing of images to that of z' -band, limiting 3σ aperture magnitude in (R, i', z') is (26.8, 27.3, 26.0) and (27.1, 27.3, 26.3) for J08 and J11 fields, respectively. We chose LBGs at $z \sim 5$ from our catalog using the criteria below (Yoshida et al. 2006):

$$R - i' > 1.0 \quad (8)$$

$$i' - z' < 0.7 \quad (9)$$

$$R - i' > 1.2(i' - z') + 0.9 \quad (10)$$

$$z' < 5\sigma_{z'}. \quad (11)$$

In Figure 3 we show color-color diagrams of J08 and J11 fields.

In Yoshida et al. (2006), the contamination rate of this $Ri'z'$ -LBG sample is estimated via Monte Carlo simulation based on photometric redshift catalog of galaxies

in the Hubble Deep Field. The derived value of $\lesssim 0.05$ is negligibly low. After visual inspection, the number of LBGs detected in J08 and J11 field is respectively 33 and 137. LBGs are also divided into “proximity” sample and “blank fields” sample as done for LAEs. The number of LBGs in proximity sample is 10 and 35 in J08 and J11 field, respectively.

3.3. Physical Properties of LAEs and LBGs

We derived $\text{Ly}\alpha$ and UV luminosity and rest-frame equivalent width (EW_0) of LAEs assuming that the UV continuum slope is flat and the i' -band and narrow-band fluxes of LAEs are expressed as

$$\begin{aligned} f_{i'} &= f_{\text{cont}} + F_{\text{Ly}\alpha}/\Delta_{i'} \\ f_{\text{NB711}} &= f_{\text{cont}} + F_{\text{Ly}\alpha}/\Delta_{\text{NB711}} \end{aligned}$$

in the J08 and J11 fields and

$$\begin{aligned} f_{i'} &= f_{\text{cont}} \\ f_{\text{NB671}} &= f_{\text{cont}} + F_{\text{Ly}\alpha}/\Delta_{\text{NB671}} \end{aligned}$$

in 4C04 field, where $F_{\text{Ly}\alpha}$ and f_{cont} respectively denote the $\text{Ly}\alpha$ flux in units of $\text{erg s}^{-1} \text{cm}^{-2}$ and the continuum flux in units of $\text{erg s}^{-1} \text{cm}^{-2} \text{\AA}^{-1}$; $f_{i'}$, f_{NB711} , and f_{NB671} respectively denote i' -, NB711 -, and NB671 -band flux in units of $\text{erg s}^{-1} \text{cm}^{-2} \text{\AA}^{-1}$; and $\Delta_{i'}$, Δ_{NB711} , and Δ_{NB671} respectively denote the FWHMs of i' -, NB711 -, and NB671 -band in units of \AA . Then $\text{Ly}\alpha$ luminosity and EW_0 of LAEs are expressed by following formula:

$$\begin{aligned} L_{\text{Ly}\alpha} &= 4\pi d_L^2 F_{\text{Ly}\alpha} \\ &= 4\pi d_L^2 \frac{\Delta_{\text{NB711}}(f_{\text{NB711}} - f_{i'})}{1 - \Delta_{\text{NB711}}/\Delta_{i'}} \end{aligned} \quad (12)$$

$$\text{or} = 4\pi d_L^2 \Delta_{\text{NB671}}(f_{\text{NB671}} - f_{i'}) \quad (13)$$

and

$$\begin{aligned} \text{EW}_0 &= F_{\text{Ly}\alpha}/f_{\text{cont}}(1+z) \\ &= \frac{\Delta_{\text{NB711}}(f_{\text{NB711}} - f_{i'})}{f_{i'} - (\Delta_{\text{NB711}}/\Delta_{i'})f_{\text{NB711}}} \frac{1}{1+z} \end{aligned} \quad (14)$$

$$\text{or} = \frac{\Delta_{\text{NB671}}(f_{\text{NB671}} - f_{i'})}{f_{i'}} \frac{1}{1+z}. \quad (15)$$

Equation 12 and 14 are used in J08 and J11 fields and Equation 13 and 15 are used in 4C04 field. UV luminosity of LBGs is directly derived from z' -band magnitude.

To derive number density and luminosity function of LAE and LBG, we have to calculate the effective volume surveyed and the completeness. These can be obtained by using Monte Carlo simulations in the same manner as done in many surveys such as Ouchi et al.

(2003) and Yoshida et al. (2006). For LAEs, we derived the effective volume by simply multiplying the surface area probed by the depth determined by the narrow-band filters we used. This gives total surveyed volume of $\sim 1.5 \times 10^5$ cMpc³ for J08 & J11 fields and 2.9×10^5 cMpc³ for 4C04 field². When we calculate the LAE completeness, we used colors of LAEs with $> 5\sigma$ detection in the i' -band as artificial LAEs. We randomly distributed artificial point sources in the real images. Then we ran SExtractor and applied the same selection criteria to them as the real sample constructions. The completeness is defined as a ratio of the number of reproduced objects that again passed the criteria to the number of all of the input objects in unmasked regions. Completeness ($C_{\text{NB}}(m_{\text{NB}})$) correction was done by weighting a LAE which has NB magnitude m_{NB} by $1/C_{\text{NB}}(m_{\text{NB}})$. This simple method gives sufficiently reliable estimates (Shimasaku et al. 2006). Note that our main purpose here is to compare the relative shape of luminosity functions in and out of the proximity and not to compare the absolute values of them. On the other hand, the effective volume and completeness of LBGs cannot be obtained immediately. We derive the effective surveyed volume $V_{\text{eff}}(m)$ as follows:

$$\begin{aligned} V_{\text{eff}}(m) &= \int_0^\infty C(m, z) \frac{dV_C(z)}{dz} dz \\ &= \int_0^\infty C(m, z) \frac{c}{H_0 E(z)} d_c^2 d\Omega dz \quad (16) \end{aligned}$$

where $C(m, z)$ is the completeness of a LBG at redshift z with apparent magnitude of m ; $V_C(z)$ is a comoving volume at redshift z ; d_C is comoving distance; and $E(z) \equiv \sqrt{\Omega_m(1+z)^3 + \Omega_\Lambda}$. The completeness $C(m, z)$ is calculated in a similar way to Yoshida et al. (2006): we generate mock LBGs using the stellar population synthesis model of Bruzual & Charlot (2003) with varying dust extinction ($E(B - V) = 0.0\text{--}0.5$, $\Delta E(B - V) = 0.1$, adopting Calzetti’s extinction law (Calzetti et al. 2000)). The distribution of $E(B - V)$ values is taken from that of $z \sim 4$ LBGs measured in Ouchi et al. (2004). Age and metallicity are kept to the constant value of 0.1 Gyr and $0.2Z_\odot$, respectively. We used an exponentially decaying star formation history with the e-folding time of 5 Gyr. After redshifting the spectra to $z = 4.4\text{--}5.3$, we corrected for the effect of intergalactic absorption by neutral hydrogen by adopting the model of Madau (1995). Then we derive the colors of the model LBGs and input them as point sources into the real images. Source detection and photometry were

done in the same manner as in the real sample constructions. Finally, we derived the completeness as functions of z' -band magnitude and redshift.

4. RESULTS AND DISCUSSION

4.1. Environments of high-redshift AGNs

We show in Figure 4 the sky distributions of the central AGNs, LAEs and LBGs (J08 & J11 fields only) selected in Section 3.1 and 3.2. The two QSOs are located close to the local peaks of surface density, while the RG is isolated. The significance of the peaks near the QSOs is lower than 2σ in either case. This level of variance is found in other blank field surveys (Ouchi et al. 2003, 2005; Shioya et al. 2009). Chiang et al. (2013) derived median and 1σ scatter of overdensities of galaxies with $\text{SFR} > 1 M_\odot/\text{yr}$, $\delta_{\text{gal}} \equiv (n - \bar{n})/\bar{n}$ (see their Figure 13 for $z = 3$ case) as a function of Δz by using a semi-analytic model. In our cases δ_{gal} is at most ~ 1 . Note that the area of the window of 15×15 cMpc used in Chiang et al. (2013) is close to our aperture size (circle of 8 cMpc radius). At least they are not likely to be associated with the most massive overdensity at $z \sim 5$ or evolve into ‘‘Coma’’ type clusters with $M_{\text{halo}} > 10^{15} M_\odot$, though there remains the possibility of them being ‘‘Fornax’’ type cluster ($M_{\text{halo}} < 3 \times 10^{14} M_\odot$). Though the density peak of LBGs in J08 field is also near J08 itself, the distribution of LBGs as a whole is clearly different from that of LAEs.

The trend of no massive overdensity becomes clearer in Figure 5 and 6, in which we respectively show the Ly α luminosity functions (LFs) of LAEs and UV LFs of LBGs in each field. The error bars represent 84% single-sided confidence levels based on the Poisson statistics (Gehrels 1986) alone. We find no significant excess of LFs in the proximities compared to that in blank fields. Rather, we find no LAEs in the two brightest bins in the proximities of the two QSOs at $z \sim 4.9$. We also find no LBG in the two brightest bins and the brightest bin in J08 and J11 field, respectively. This is reasonable considering the small volume probed and the smaller number density of brighter LAEs and LBGs. Indeed, if we assume that the number of these galaxies follows the Poisson distribution and that the surface density of galaxies in the proximity are the same as that in the outer region, the probability of finding no LAEs with $L_{\text{Ly}\alpha} > 10^{42.75}$ (and LBGs with $M_{\text{UV}} < -21.6$) in the proximity of J08 and J11 is 36% and 14% (36% and 10%), respectively. These threshold values correspond to those of the second brightest bin in the LFs in Figure 5 and 6. On the other hand, if we assume the surface density of LAEs (LBGs) in the QSO proximity is twice as high as blank fields, probabilities of non-detection de-

² These values include the masked regions. The masked regions are at most 10% and thus negligibly small.

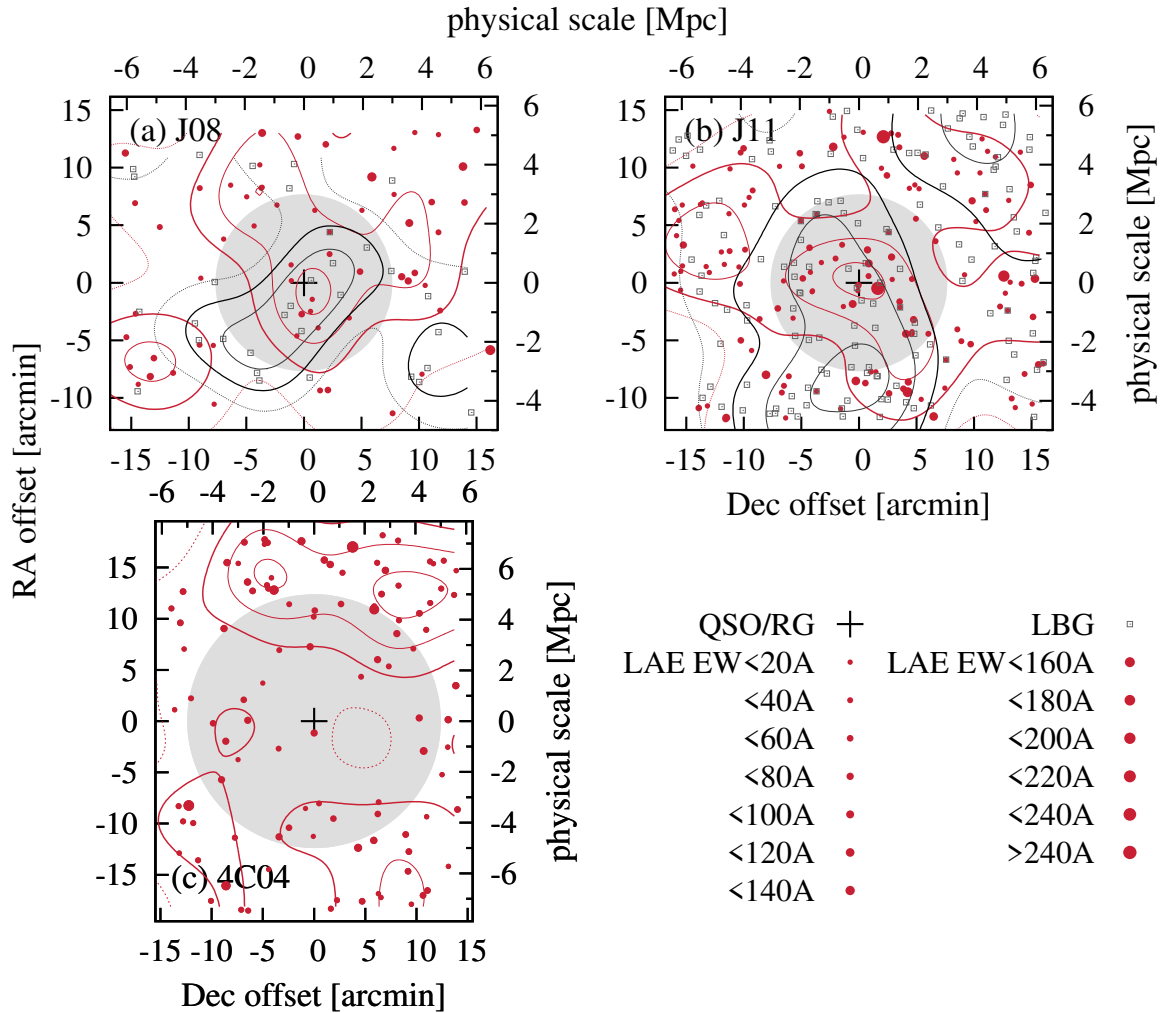


Figure 4. Sky distribution of LAEs in (a) J08, (b) J11, and (c) 4C04 field. The plus signs at the center denote the location of the AGNs. Filled red circles denote LAEs. The size of the circles depends on $\text{Ly}\alpha$ EW₀. Filled gray squares denote LBGs. The gray shaded areas show the proximity of 3 pMpc (J08 and J11 fields) or 5 pMpc (RG field) centered at each AGN. Red and black contours indicate surface density $\delta_{\text{gal}} \equiv (n - \bar{n})/\bar{n}$ of LAEs and LBGs (including QSO/RG) from 1.0 to -0.5 with a step of 0.5 in the case of J08 and 4C04 and 0.8 to -0.8 with a step of 0.4 in the case of J11, derived by the fixed aperture method; we distributed apertures of radius 8 cMpc and counted the number of galaxies within them ($\equiv n$), and derived the average ($\equiv \bar{n}$) in each field. Thick solid lines indicate $\delta_{\text{gal}} = 0$ and dotted lines show negative δ_{gal} . Note, however, that number density at the edge of each field is underestimated and contours are plotted just to guide the eye.

crease to 13% and 1.9% (13% and 1.1%), respectively. As we discuss further in section 4.2, the impact of AGN feedback seems to be negligible in our data; even at the fainter side, there is no significant difference. This trend holds true for the case of LBGs (Figure 6), which suggests that these QSOs do not reside in overdensities of much larger scales considering large Δz of the LBG selection function.

The RG 4C04 is found to be near a void. The number density of LAEs in the proximity of the RG is somewhat lower than in the outer region. This is at odds with the results in the literature (Zheng et al. 2006; Ajiki et al. 2006; Venemans et al. 2007), in which the authors report overdensity of LAEs around radio-loud

QSOs and RGs at various redshifts with a high success rate ($\gtrsim 70\%$). We note that 4C04 has extremely luminous ($L_{\text{Ly}\alpha} > 10^{44}$ erg s⁻¹) and extended ($\gtrsim 60$ kpc) $\text{Ly}\alpha$ halo around it (Figure 7). High redshift RGs (HzRGs) often have such extended $\text{Ly}\alpha$ halos. They usually align with their radio jets (Venemans et al. 2007; Nesvadba et al. 2016). However, the 4C04 halo is rather extended almost perpendicular to the jet direction (arrows in Figure 7). The $\text{Ly}\alpha$ nebula extending far beyond the radio emitting region, and the non-detection of overdensity and the C IV and He II lines (Kopylov et al. 2006) which are frequently detected in HzRGs with line ratios suggestive of an enriched outflow origin, all suggest that this RG is a different class of objects from other

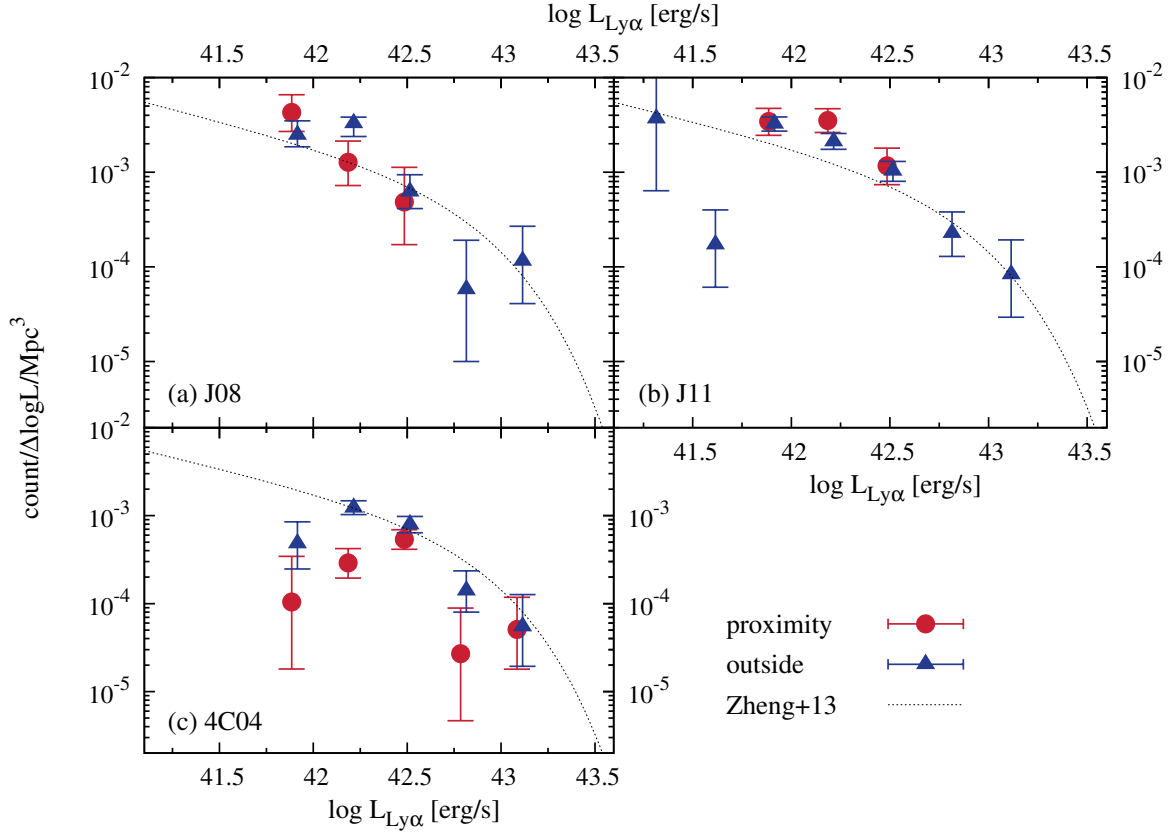


Figure 5. Ly α luminosity functions of LAEs in (a) J08, (b) J11, and (c) 4C04 field. Red circles and blue triangles respectively represent LFs in the proximity and in the outer region. The dotted line is a LF of LAE at $z \sim 4.5$ derived in Zheng et al. (2013) using spectroscopically confirmed LAEs with $L_{\text{Ly}\alpha} > 10^{42.5}$.

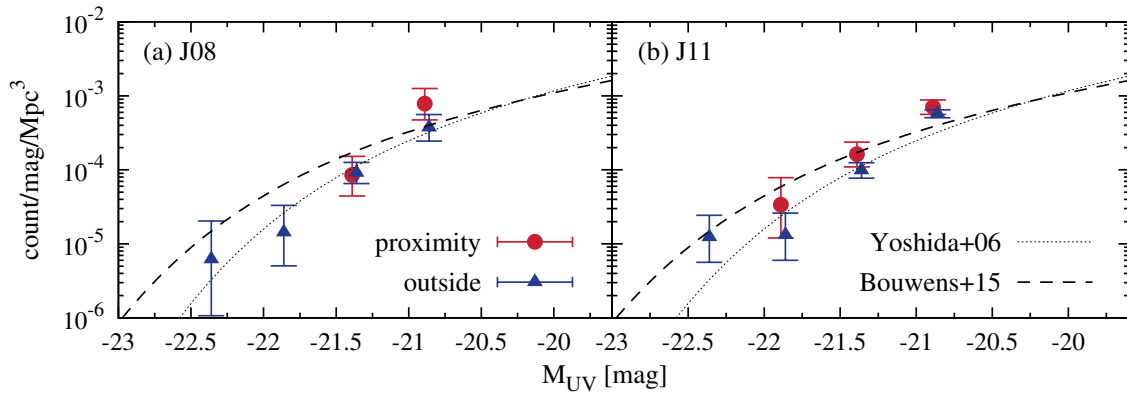


Figure 6. UV luminosity functions of LBGs in (a) J08 and (b) J11 field. Red circles and blue triangles respectively represent LFs in the proximity and in the outer region. The dotted and dashed lines are respectively the LFs at $z \sim 5$ derived in Yoshida et al. (2006) and Bouwens et al. (2015). These papers use different selection criteria to select galaxies at $z \sim 5$. Our selection criteria are the same as those used in Yoshida et al. (2006).

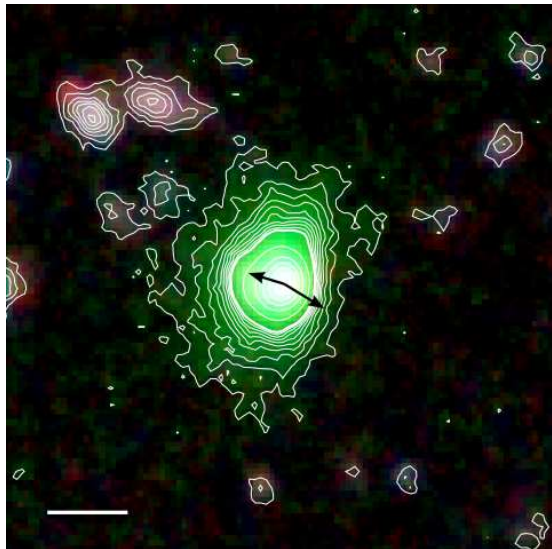


Figure 7. Pseudo-color image of 4C04 with north to right and east to up. R, G, and B correspond to i' -, $NB671$ -, and R -band, respectively. Contour level is different above and below the thick line ($6.1 \times 10^{-17} \text{ erg s}^{-1} \text{ cm}^{-2} \text{ arcsec}^{-2}$) for clarity: the step size outside of the thick line corresponds to $6.1 \times 10^{-18} \text{ erg s}^{-1} \text{ cm}^{-2} \text{ arcsec}^{-2}$ and the step size inside the thick line is 20 times larger than outside. The scale bar at the bottom left of the figure indicates 20 pkpc ($\sim 3''$). The size of the image is $20'' \times 20''$. The black arrows indicate the direction of a radio jet and the location of bright lobes in Parijskij et al. (2014).

HzRGs. Additionally, though the upper limit of the line ratios of the halo are consistent with bright (type-1) QSOs (Borisova et al. 2016), the moderately broad $\text{Ly}\alpha$ line width ($\sim 1500 \text{ km/s}$, Kopylov et al. 2006) is not consistent with those QSOs. Further observations are needed to conclude the origin of this $\text{Ly}\alpha$ nebula.

Considering a large scatter in the number of galaxies even with Suprime-Cam FoV (can be as large as ~ 0.3 depending on the bias factor of LAEs, e.g. Shimasaku et al. 2004; Gawiser et al. 2007; Trenti & Stiavelli 2008), it is hard to draw a firm conclusion from our observations alone. Nonetheless, observing more and more AGN fields with small Δz and comparing the results with theories greatly help us understand the true nature of AGN environments. Besides our results, there is growing observational evidence that high-redshift ($z \gtrsim 5$) AGNs do not reside in overdensities when one probes them with narrow-band filters ($\Delta z \lesssim 0.1$) at least on a scale smaller than 3 pMpc (Bañados et al. 2013; Mazzucchelli et al. 2017 at $z = 5.7$). These results suggest that an overdensity on this scale (and possibly galaxy merger) is not always a necessary condition for AGN activity. Some semi-analytic models predict that halos of high-redshift AGNs are not

the most massive ones at that epoch (Overzier et al. 2009; Fanidakis et al. 2013; Orsi et al. 2016). Recently Di Matteo et al. (2016) suggested that the most massive BHs at the earliest epoch ($z > 8$) can be preferentially formed in regions where tidal fields are weak because gas can directly fall onto BHs along filaments, rather than mere overdense regions. On the other hand, Costa et al. (2014) argued that SMBHs of $10^9 M_{\odot}$ at $z \sim 6$ only formed in the most massive halos as a result of their cosmological hydrodynamical simulations. The environments identified in theoretical works depend largely on their assumptions about BH seeding, BH growth, and AGN feedback. For example, models usually assume that AGNs are triggered only by galaxy-galaxy mergers. Furthermore, we have to rely on simple subgrid physics because nuclear regions are impossible to resolve in galaxy scale simulations. Clearly models need to be tested and updated with recent observational indications. Although AGN luminosity is still important in terms of AGN feedback, it is also crucial to investigate the AGN environment as a function of BH mass. This is because AGN luminosity is rather an instantaneous, time-changing (“differential”) physical quantity determined by SMBH mass and accretion rate at the observed time. On the other hand, BH mass is a more fundamental “cumulative” one which reflects its growth history and thus more likely to be related to its large scale environments.

Finally, we mention another possibility: we failed to trace the environments with LAEs and LBGs because, for example, most of galaxies around AGNs may be dusty and UV/optically elusive. Many lines of evidence suggest that LAEs are typically young ($\lesssim 100 \text{ Myr}$), low-mass ($\lesssim 10^8 M_{\odot}$) and non-dusty ($E(B - V) \lesssim 0.2$) galaxies (Gawiser et al. 2006; Ono et al. 2010a,b; Finkelstein et al. 2007, 2009) with some massive and dusty outliers. As there are many systems with a large amount of dust even at this high redshift (Riechers et al. 2013), we could largely miss such a population. Recently, Trakhtenbrot et al. (2017) observed six $z \sim 4.8$ QSOs from the same parent sample we used with ALMA and detected companion SMGs in three of the observed AGNs. High probability of finding companion SMGs in a small FoV of ALMA and faintness of the companions in other wavelengths (not detected even in the Spitzer data) indicate that there may be many optically-elusive galaxies around AGNs in our fields. Since the techniques utilizing UV/optical feature are biased against dust obscured galaxies, wide-field (far-)infrared observations are needed to complement such techniques.

4.2. Feedback from AGNs

It has long been theoretically argued that ultraviolet background (UVB) radiation can suppress the formation of low-mass galaxies by heating their gas (Efstathiou 1992; Thoul & Weinberg 1996; Kitayama et al. 2000, 2001; Benson et al. 2002; Dijkstra et al. 2004; Susa & Umemura 2004; Mesinger & Dijkstra 2008; Okamoto et al. 2008; Sobacchi & Mesinger 2013a,b; Liu et al. 2016). In principle, we can confirm this suppression by identifying flattening of the faint-end slope of the LF, though observationally this turned out to be extremely difficult (Weisz et al. 2014; Alavi et al. 2014, 2016; Castellano et al. 2016); no evidence of an LF turnover has been found down to $M_{UV} \sim -12$. On the other hand, there are a handful of candidate ultra-faint dwarf galaxies at the local Universe (Brown et al. 2014, $M_V > -8$ or $M_* \lesssim 10^4 M_\odot$) whose star-formation seem to have been suppressed by a synchronized external process such as the reionization. This kind of negative feedback is often provoked to explain why we do not always find high-redshift QSOs in overdensities because local UV radiation fields around luminous QSOs are much stronger than the UVB. Previous studies originally considered situations where a pregalactic cloud is collapsing under UVB in the reionization era and studied its evolution as a function of various parameters such as the intensity of UVB, the time at which UVB is switched on and the pregalactic cloud starts to collapse (see also Kashikawa et al. 2007). As a result, they derived the threshold dynamical mass below which a pregalactic cloud cannot collapse and form stars. The results showed a range of the threshold mass of $\sim 10^9$ – $10^{10} M_\odot$, depending on the details of calculations (e.g., 1D/3D, including radiative transfer effect or not.). They also found that once the clouds begin to collapse and their density get higher, even very strong UV radiation cannot affect the evolution of the clouds and finally allows the clouds to form stars, whereas clouds which are irradiated well before they start to collapse can be affected significantly (Kashikawa et al. 2007; Sobacchi & Mesinger 2013b; Roos et al. 2015). In many cases the strength of UVB is kept constant, but in some cases gradually evolving UVB is assumed. The impact of UVB feedback is maximized when clouds are irradiated by constant UVB before they begin to collapse.

Although the assumptions in the above theoretical studies are not exactly matched to the situation studied in this paper (i.e., UVB vs. the AGN proximity), we can refer to these results to infer in what circumstances the impact of radiative AGN feedback becomes significant. First, a semi-analytic model predict halo masses of faint ($10^{41} < L_{Ly\alpha} < 10^{42} \text{ erg s}^{-1}$) LAEs,

moderate-luminosity ($10^{42} < L_{Ly\alpha} < 10^{43} \text{ erg s}^{-1}$) LAEs, and LGBs with UV magnitude brighter than $M_{UV} = -20.8$ at $z \sim 5$ of $\sim 10^{10.4} M_\odot$, $10^{11.1} M_\odot$, and $10^{11.7} M_\odot$, respectively (Garel et al. 2015). Halo mass of faint LAE is in agreement with the threshold mass. Second, the strength of UV radiation field at 3 pMpc from our QSOs is stronger than that of UVB at $z \sim 5$. It is parametrized as $J(\nu) = J_{21} \times (\nu/\nu_0)^\alpha \times 10^{-21} \text{ erg s}^{-1} \text{ Hz}^{-1} \text{ cm}^{-2} \text{ sr}^{-1}$, where ν_0 denotes the Lyman limit frequency and α denotes continuum slope. We derive J_{21} at 3 pMpc from the QSOs assuming UV continuum slope $\alpha = -0.99$ (Fan et al. 2001) and using the measured luminosity at 1450Å, L_{1450} from Trakhtenbrot et al. (2011), to find $J_{21} = 1.2$ and 0.7 for J08 and J11, respectively. Inferred UVB radiation J_{21} at $z \sim 5$ is of order 0.1 (Calverley et al. 2011) and is similar to the assumed value in previous calculations which predict strong feedback. Thus, taken at face value, fainter LAEs in our sample can be significantly affected by those QSOs.

However, there are some caveats in the above arguments. First, in order to suppress the formation of LAEs significantly, QSOs should be switched on before LAEs around them starts to form. This can be the case if the lifetime of the QSO phase is similar to an estimated maximum value of $\sim 10^8$ – 10^9 yr (Marconi et al. 2004), since estimated age of LAEs is \sim a few $\times 1$ –100 Myr (Finkelstein et al. 2009). Second, the short time-scale variability of the UV source is not taken into account in the theories. QSOs show strong variability on timescales as short as days. At the same time, many simulations showed that AGNs change their luminosity dramatically in the course of major mergers and also there are some indications of AGN flickering on timescales $\sim 10^5$ yr (Schawinski et al. 2015). If the variability is taken into account, the impact of AGN feedback is further weakened because high-redshift AGNs probed so far are considered to be near its peak luminosity and its time-averaged luminosity may be lower (Hopkins et al. 2006; Hopkins & Hernquist 2009). Third, although primordial gas is assumed in the calculations, pregalactic clouds can contain metals and dust grains which do not originate from in situ star formation but from neighboring galaxies via various mechanisms such as galactic winds and radiation pressure. This makes cooling and heating processes more complex: metals (Wiersma et al. 2009) and dust emission contribute cooling once the temperature and density get high enough ($> 10^6$ K) and make star formation easier, whereas photoelectric dust heating could be quite efficient and negative feedback could be stronger at the temperature, UVB strength, and den-

sity condition of the earlier stage of collapse considered here (Nath et al. 1999; Montier & Giard 2004).

Though the effect of metals and dusts is unknown, if a QSO activates well before surrounding galaxies start to collapse, and retains its high luminosity for 10^8 – 10^9 years, the suppression of faint galaxies due to a QSO can be observable. These conditions may not be always fulfilled (e.g., there are many works claiming an episodic and short QSO phase; see Martini 2003). Even if it exists, only LAEs fainter than $L_{\text{Ly}\alpha} = 10^{42}$ erg s $^{-1}$ and LBGs fainter than $M_{\text{UV}} = -18.3$ seem to be critically affected. Since limiting magnitudes of observations conducted in the past are much brighter, it is difficult to explain the deficit of overdensity around QSOs reported so far by radiative feedback, unless halo masses of LAEs are overestimated. More realistic calculations and much deeper observations are clearly needed to qualitatively examine AGN radiative feedback.

4.3. Fluorescent emission

High-EW LAEs are interesting because such high Ly α EW (> 240 Å) is unlikely to be due solely to normal star formation (Charlot & Fall 1993; Schaerer 2003). It is usually attributed to clumpy, dusty IGM (Hansen & Oh 2006; Finkelstein et al. 2008; Kobayashi et al. 2010) or fluorescent Ly α emission (Adelberger et al. 2006; Cantalupo et al. 2005, 2007) especially in the case of QSO environments. Cantalupo et al. (2012) reported that many Ly α fluorescent systems illuminated by a hyperluminous QSO at $z = 2.4$ are clustered around the QSO and argued that, as opposed to the case of feedback (Section 4.2), the fainter-side of Ly α LF of LAEs around the QSO becomes steeper due to these sources. In our sample, only two LAEs in J11 field have such high EW. One of the LAEs is located at ~ 0.7 pMpc (projected) from J11. The other is located at ~ 5 pMpc (projected) from J11. Though the former can be significantly affected by radiation from the QSO, the latter are unlikely to be significantly affected, since at that distance QSO radiation is comparable to UVB. Cantalupo et al. (2012) predicted that if fluorescence is dominant in the field, $L_{\text{Ly}\alpha}$ of LAEs should decrease with increasing distance from the QSO. Figure 8 shows the number, Ly α equivalent widths (EWs) and Ly α luminosities of LAEs as a function of the projected distance from the central AGNs. In Panel (a), we see the possible signature of local peak seen in Figure 4, i.e., the rising trend of the number of LAEs at < 2 pMpc in J08 and J11 field. However, in Panel (b) and (c), we find no dependence on the distance in any field. This suggests that the properties of most of the LAEs in these fields are not affected by the central AGNs.

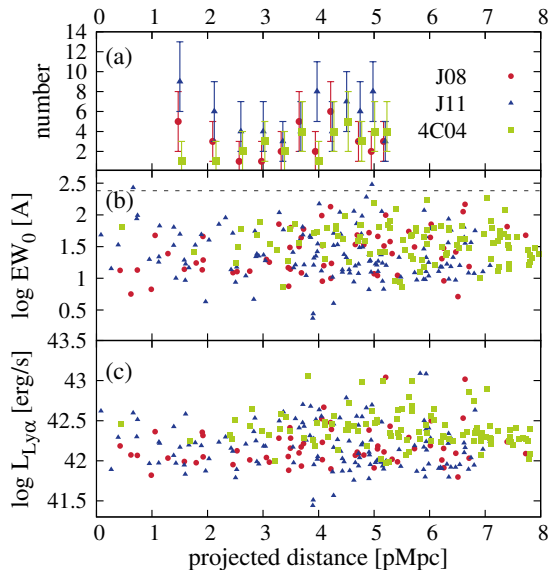


Figure 8. Properties of LAEs as a function of the projected distance from the central AGNs. (a): The number of LAEs with $L_{\text{Ly}\alpha} > 10^{42}$ erg s $^{-1}$ in annuli centered at J08 (Red circles), J11 (Blue triangles), and 4C04 (Green squares). Widths of annuli was chosen so that each annulus has the same area. (b): Rest-frame equivalent width. A horizontal dashed line represent EW of 240 Å. (c): Ly α luminosity of LAEs.

There is one interesting source in the J11 field: a close companion LAE located at 80 pkpc away from J11. We show the pseudo-color image **and the continuum-subtracted Ly α image** of J11 and the companion in Figure 9. **The companion clearly shows a Ly α halo which extends toward the QSO direction** and may suggest interactions between these two galaxies. Though Δz of *NB711* filter is large compared to 80 pkpc, if the companion is at the same redshift as J11, J_{21} will be ~ 1000 . Following Cantalupo et al. (2005), we derived the “effective boost factor” b_{eff} to be ~ 3000 . Thus if there exist optically thick clouds, they can be detected with our imaging observations. Ly α luminosity of the QSO near side is ~ 1.8 times that of the far side. Thus, although EW is not high ($\text{EW}_0 \sim 48$ Å), fluorescent emission may contribute to its $L_{\text{Ly}\alpha}$, if not all. We also note that the QSO J11 itself showed asymmetric, extended Ly α emission toward the opposite side of the companion. This may imply a giant filamentary structure passing through these two galaxies. Confirming this issue needs further observations and will be discussed elsewhere.

5. SUMMARY AND CONCLUSIONS

High-redshift AGNs are thought to be signposts of highly biased regions of the Universe. Previous studies on their environments though presented confusing re-

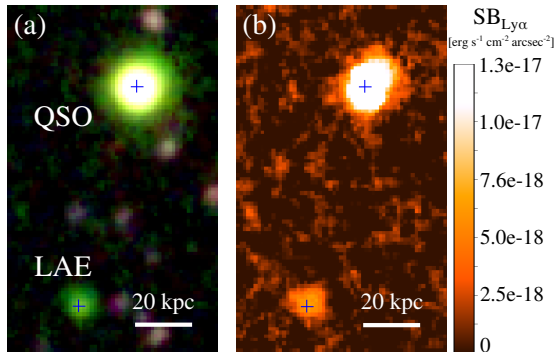


Figure 9. Pseudo-color image of J11 and the close companion marked respectively as “QSO” and “LAE” (Panel (a)) and Ly α image (Panel (b)). The scale bar at bottom right of the figure indicates 20 pkpc ($\sim 3''$). The size of this panel is $20'' \times 12''$. The plus signs show the location of the i' -band peak of each source. In Panel (a), R, G, and B correspond to i' -, $NB711$ -, and R -band, respectively. In Panel (b), extended Ly α halos around both sources can be seen.

sults, suggesting that AGNs reside in both rich and poor environments. This is partly due to the use of different techniques and possibly radiative feedback from AGNs. The conventional Lyman-break technique only gives us an unclear picture because it selects galaxies from wide redshift range ($\Delta z \sim 1$, corresponds to ~ 100 physical Mpc at the redshift of interest of this study, $z \sim 5$), making it difficult to discuss local (a few-several physical Mpc, corresponds to $\Delta z \sim 0.1$) environments around AGNs. In order to test whether AGN environments are rich and whether AGN feedback is indeed strong enough to suppress formation of neighboring galaxies, we conducted deep and wide-field imaging observations with the Suprime-Cam on the Subaru telescope and searched for LAEs around two QSOs at $z \sim 4.9$ and an RG at $z \sim 4.5$ by using narrow-band filters. In QSO fields, we also obtained additional broad-band images to select LBGs at $z \sim 5$ for comparison. We constructed a photometric sample of 301 LAEs and 170 LBGs in total. A wide field of view ($34' \times 27'$) of the Suprime-Cam enabled us to probe these galaxies in the immediate vicinities of the AGNs and in the blank fields simultaneously and compare various properties of them in a consistent manner. We find that the QSOs are located near low peaks of galaxy surface density, though the data suggest they are not uncommon (with $< 2\sigma$ significance), and one of the QSOs has a close companion LAE with projected distance ~ 80 physical kpc. However, the luminosity functions of LAE/LBG around the QSOs and RG are consistent with or lower than those in blank fields as opposed to the expectation that they should reside in the most massive overdensities. Moreover, we find no

evidence of feedback even in the faintest luminosity bin (down to $L_{\text{Ly}\alpha} = 10^{41.8} \text{ erg s}^{-1}$).

Through our discussion in Section 4.2, we conclude that radiative feedback is unlikely to affect our sample and galaxies around high-redshift AGNs observed to date. Therefore our results suggest that high-redshift AGNs do not necessarily trace overdense regions of the Universe and that is not due to radiative feedback. Note that most of the currently known QSO fields with significant overdensity of neighboring galaxies are detected with LBGs, and that spectroscopic follow-up of them is very challenging with the existing instruments. Thus there still remains a possibility that the photometric sample around those overdense regions is significantly affected by the projection effect. Further observations with narrow-band filters around high-redshift AGNs are the best way to know the true nature of their environments. In parallel, observations around them with submillimeter/millimeter facilities like ALMA (Trakhtenbrot et al. 2017) is crucial for detecting possible dusty galaxies. Large-area surveys will find more and more AGNs at high-redshift with their redshifted Ly α emission line falling into the existing narrow-band filters. For example, many narrow-band filters are installed on the Hyper Suprime-Cam (Miyazaki et al. 2012), which has much wider FoV (1.5 degrees in diameter) than the Suprime-Cam and thus is the most powerful instrument for this study. Particularly, Subaru High- z Exploration of Low-Luminosity Quasars (SHELLQs; Matsuoka et al. 2016) will find many high-redshift low-luminosity QSOs, including QSOs with very massive SMBHs but with low accretion rate, and will help us reveal more general trends of high-redshift AGN environments.

We greatly appreciate the anonymous referee for his/her thoughtful comments. We thank Tomonori Totani and Nobunari Kashikawa for helpful comments and discussions. We would like to appreciate all the staffs who supported our observations with the Subaru Telescope, including the staffs of the National Astronomical Observatory of Japan, Mauna Kea Observatory, and local Hawaiian people who have been making effort to preserve and share the beautiful dark sky of Mauna Kea with us. MI is supported by JSPS KAKENHI Grant Number 15K05030. YM is supported by JSPS KAKENHI Grant Number 17H04831. KS is supported by JSPS KAKENHI Grant Number 16K05286.

Facilities: Subaru(Suprime-Cam)

Software: SDFRED2, L.A.Cosmic, SExtractor, IRAF

REFERENCES

- Adams, S. M., Martini, P., Croxall, K. V., Overzier, R. A., & Silverman, J. D. 2015, *Monthly Notices of the Royal Astronomical Society*, 448, 1335
- Adelberger, K. L., Steidel, C. C., Kollmeier, J. A., & Reddy, N. A. 2006, *The Astrophysical Journal*, 637, 74
- Ajiki, M., Taniguchi, Y., Murayama, T., et al. 2006, *Publications of the Astronomical Society of Japan*, 58, 499
- Alavi, A., Siana, B., Richard, J., et al. 2014, *The Astrophysical Journal*, 780, 143
- . 2016, *The Astrophysical Journal*, 832, 56
- Bañados, E., Venemans, B., Walter, F., et al. 2013, *The Astrophysical Journal*, 773, 178
- Bechtold, J. 1994, *The Astrophysical Journal Supplement Series*, 91, 1
- Benson, A. J., Lacey, C. G., Baugh, C. M., Cole, S., & Frenk, C. S. 2002, *Monthly Notices of the Royal Astronomical Society*, 333, 156
- Bertin, E., & Arnouts, S. 1996, *Astronomy and Astrophysics Supplement Series*, 117, 393
- Boris, N. V., Sodre, Jr., L., Cypriano, E. S., et al. 2007, *The Astrophysical Journal*, 666, 747
- Borisova, E., Lilly, S. J., Cantalupo, S., et al. 2016, *The Astrophysical Journal*, 830, 120
- Bouwens, R. J., Illingworth, G. D., Oesch, P. A., et al. 2015, *The Astrophysical Journal*, 803, 34
- Brown, T. M., Tumlinson, J., Geha, M., et al. 2014, *The Astrophysical Journal*, 796, 91
- Bruns, L. R., Wyithe, J. S. B., Bland-Hawthorn, J., & Dijkstra, M. 2012, *Monthly Notices of the Royal Astronomical Society*, 421, 2543
- Bruzual, G., & Charlot, S. 2003, *Monthly Notices of the Royal Astronomical Society*, 344, 1000
- Calverley, A. P., Becker, G. D., Haehnelt, M. G., & Bolton, J. S. 2011, *Monthly Notices of the Royal Astronomical Society*, 412, 2543
- Calzetti, D., Armus, L., Bohlin, R. C., et al. 2000, *The Astrophysical Journal*, 533, 682
- Cantalupo, S., Lilly, S. J., & Haehnelt, M. G. 2012, *Monthly Notices of the Royal Astronomical Society*, 425, 1992
- Cantalupo, S., Lilly, S. J., & Porciani, C. 2007, *The Astrophysical Journal*, 657, 135
- Cantalupo, S., Porciani, C., Lilly, S. J., & Miniati, F. 2005, *The Astrophysical Journal*, 628, 61
- Capak, P. L., Riechers, D., Scoville, N. Z., et al. 2011, *Nature*, 470, 233
- Cappellari, M., Emsellem, E., Krajnović, D., et al. 2011, *Monthly Notices of the Royal Astronomical Society*, 416, 1680
- Castellano, M., Dayal, P., Pentericci, L., et al. 2016, *The Astrophysical Journal*, 818, L3
- Charlot, S., & Fall, S. M. 1993, *The Astrophysical Journal*, 415, 580
- Chiang, Y.-K., Overzier, R., & Gebhardt, K. 2013, *The Astrophysical Journal*, 779, 127
- Costa, T., Sijacki, D., Trenti, M., & Haehnelt, M. G. 2014, *Monthly Notices of the Royal Astronomical Society*, 439, 2146
- Dawson, S., Rhoads, J. E., Malhotra, S., et al. 2007, *The Astrophysical Journal*, 671, 1227
- Di Matteo, T., Croft, R. A. C., Feng, Y., Waters, D., & Wilkins, S. 2016, arXiv: 1606.08871, doi:10.1093/mnras/stx319
- Dijkstra, M., Haiman, Z., Rees, M. J., & Weinberg, D. H. 2004, *The Astrophysical Journal*, 601, 666
- Dressler, A. 1980, *The Astrophysical Journal*, 236, 351
- Efstathiou, G. 1992, *Monthly Notices of the Royal Astronomical Society*, 256, 43P
- Eftekhazadeh, S., Myers, A. D., White, M., et al. 2015, *Monthly Notices of the Royal Astronomical Society*, 453, 2779
- Falder, J. T., Stevens, J. A., Jarvis, M. J., et al. 2011, *The Astrophysical Journal*, 735, 123
- Fan, X., Strauss, M. A., Richards, G. T., et al. 2001, *The Astronomical Journal*, 121, 31
- Fanidakis, N., Macciò, a. V., Baugh, C. M., Lacey, C. G., & Frenk, C. S. 2013, *Monthly Notices of the Royal Astronomical Society*, 436, 315
- Farina, E. P., Montuori, C., Decarli, R., & Fumagalli, M. 2013, *Monthly Notices of the Royal Astronomical Society*, 431, 1019
- Ferrarese, L., & Merritt, D. 2000, *The Astrophysical Journal*, 539, L9
- Finkelstein, S. L., Rhoads, J. E., Malhotra, S., & Grogin, N. 2009, *The Astrophysical Journal*, 691, 465
- Finkelstein, S. L., Rhoads, J. E., Malhotra, S., Grogin, N., & Wang, J. 2008, *The Astrophysical Journal*, 678, 655
- Finkelstein, S. L., Rhoads, J. E., Malhotra, S., Pirzkal, N., & Wang, J. 2007, *The Astrophysical Journal*, 660, 1023

- Francis, P. J., & Bland-Hawthorn, J. 2004, *Monthly Notices of the Royal Astronomical Society*, 353, 301
- Garcia-Vergara, C., Hennawi, J. F., Barrientos, L. F., & Rix, H.-W. 2017, arXiv: 1701.01114
- Garel, T., Blaizot, J., Guiderdoni, B., et al. 2015, *Monthly Notices of the Royal Astronomical Society*, 450, 1279
- Gawiser, E., van Dokkum, P. G., Gronwall, C., et al. 2006, *The Astrophysical Journal*, 642, L13
- Gawiser, E., Francke, H., Lai, K., et al. 2007, *The Astrophysical Journal*, 671, 278
- Gehrels, N. 1986, *The Astrophysical Journal*, 303, 336
- Gunn, J. E., & Stryker, L. L. 1983, *The Astrophysical Journal Supplement Series*, 52, 121
- Hansen, M., & Oh, S. P. 2006, *Monthly Notices of the Royal Astronomical Society*, 367, 979
- Hennawi, J. F., Prochaska, J. X., Cantalupo, S., & Arrighi-Battaia, F. 2015, *Science*, 348, 779
- Hewett, P. C., & Wild, V. 2010, *Monthly Notices of the Royal Astronomical Society*, 405, 2302
- Hopkins, P. F., & Hernquist, L. 2009, *The Astrophysical Journal*, 698, 1550
- Hopkins, P. F., Somerville, R. S., Hernquist, L., et al. 2006, *The Astrophysical Journal*, 652, 864
- Husband, K., Bremer, M. N., Stanway, E. R., et al. 2013, *Monthly Notices of the Royal Astronomical Society*, 432, 2869
- Kashikawa, N., Kitayama, T., Doi, M., et al. 2007, *The Astrophysical Journal*, 663, 765
- Kim, S., Stiavelli, M., Trenti, M., et al. 2009, *The Astrophysical Journal*, 695, 809
- Kitayama, T., Susa, H., Umemura, M., & Ikeuchi, S. 2001, *Monthly Notices of the Royal Astronomical Society*, 326, 1353
- Kitayama, T., Tajiri, Y., Umemura, M., Susa, H., & Ikeuchi, S. 2000, *Monthly Notices of the Royal Astronomical Society*, 315, L1
- Kobayashi, M. A. R., Totani, T., & Nagashima, M. 2010, *The Astrophysical Journal*, 708, 1119
- Komatsu, E., Dunkley, J., Nolta, M. R., et al. 2009, *The Astrophysical Journal Supplement Series*, 180, 330
- Kopylov, a. I., Goss, W. M., Pariski, Y. N., et al. 2006, *Astronomy Letters*, 32, 433
- Liu, C., Mutch, S. J., Angel, P. W., et al. 2016, *Monthly Notices of the Royal Astronomical Society*, 462, 235
- Madau, P. 1995, *The Astrophysical Journal*, 441, 18
- Magorrian, J., Tremaine, S., Richstone, D., et al. 1998, *The Astronomical Journal*, 115, 2285
- Marconi, A., Risaliti, G., Gilli, R., et al. 2004, *Monthly Notices of the Royal Astronomical Society*, 351, 169
- Martini, P. 2003, *Coevolution of Black Holes and Galaxies*, from the Carnegie Observatories Centennial Symposia. Published by Cambridge University Press, as part of the Carnegie Observatories Astrophysics Series., 1, 169
- Matsuda, Y., Nakamura, Y., Morimoto, N., et al. 2009, *Monthly Notices of the Royal Astronomical Society: Letters*, 400, L66
- Matsuda, Y., Richard, J., Smail, I., et al. 2010, *Monthly Notices of the Royal Astronomical Society: Letters*, 403, 54
- Matsuoka, Y., Onoue, M., Kashikawa, N., et al. 2016, *The Astrophysical Journal*, 828, 26
- Mazzucchelli, C., Bañados, E., Decarli, R., et al. 2017, *The Astrophysical Journal*, 834, 83
- Mesinger, A., & Dijkstra, M. 2008, *Monthly Notices of the Royal Astronomical Society*, 390, 1071
- Miyazaki, S., Komiyama, Y., Sekiguchi, M., et al. 2002, *Publications of the Astronomical Society of Japan*, 54, 22
- Miyazaki, S., Komiyama, Y., Nakaya, H., et al. 2012, in *Proc. SPIE*, Vol. 8446, Ground-based and Airborne Instrumentation for Astronomy IV, 84460Z
- Moehler, S., Modigliani, A., Freudling, W., et al. 2014, *Astronomy & Astrophysics*, 568, A9
- Montier, L. A., & Giard, M. 2004, *Astronomy and Astrophysics*, 417, 401
- Morselli, L., Mignoli, M., Gilli, R., et al. 2014, *Astronomy & Astrophysics*, 568, A1
- Mortlock, D. J., Warren, S. J., Venemans, B. P., et al. 2011, *Nature*, 474, 616
- Nath, B. B., Sethi, S. K., & Shchekinov, Y. 1999, *Monthly Notices of the Royal Astronomical Society*, 303, 1
- Nesvadba, N., De Breuck, C., Lehnert, M. D., Best, P. N., & Collet, C. 2016, arXiv: 1610.02057, doi:10.1051/0004-6361/201528040
- Okamoto, T., Gao, L., & Theuns, T. 2008, *Monthly Notices of the Royal Astronomical Society*, 390, 920
- Oke, J. B. 1990, *The Astronomical Journal*, 99, 1621
- Ono, Y., Shimasaku, K., Dunlop, J., et al. 2010a, *The Astrophysical Journal*, 724, 1524
- Ono, Y., Ouchi, M., Shimasaku, K., et al. 2010b, *Monthly Notices of the Royal Astronomical Society*, 402, 1580
- Orsi, Á., Fanidakis, N., Lacey, C. G., & Baugh, C. M. 2016, *Monthly Notices of the Royal Astronomical Society*, 456, 3827
- Ouchi, M., Shimasaku, K., Furusawa, H., et al. 2003, *The Astrophysical Journal*, 582, 60
- Ouchi, M., Shimasaku, K., Okamura, S., et al. 2004, *The Astrophysical Journal*, 611, 660
- Ouchi, M., Shimasaku, K., Akiyama, M., et al. 2005, *The Astrophysical Journal*, 620, L1

- Overzier, R. A. 2016, *The Astronomy and Astrophysics Review*, 24, 14
- Overzier, R. A., Guo, Q., Kauffmann, G., et al. 2009, *Monthly Notices of the Royal Astronomical Society*, 394, 577
- Parijskij, Y. N., Thomasson, P., Kopylov, A. I., et al. 2014, *Monthly Notices of the Royal Astronomical Society*, 439, 2314
- Rhoads, J. E., Malhotra, S., Dey, A., et al. 2000, *The Astrophysical Journal*, 545, L85
- Riechers, D. A., Bradford, C. M., Clements, D. L., et al. 2013, *Nature*, 496, 329
- Roos, O., Juneau, S., Bournaud, F., & Gabor, J. M. 2015, *The Astrophysical Journal*, 800, 19
- Sandrinelli, A., Falomo, R., Treves, A., Farina, E. P., & Uslenghi, M. 2014, *Monthly Notices of the Royal Astronomical Society*, 444, 1835
- Schaerer, D. 2003, *Astronomy and Astrophysics*, 397, 527
- Schawinski, K., Koss, M., Berney, S., & Sartori, L. F. 2015, *Monthly Notices of the Royal Astronomical Society*, 451, 2517
- Schlegel, D. J., Finkbeiner, D. P., & Davis, M. 1998, *The Astrophysical Journal*, 500, 525
- Shen, Y., Strauss, M. A., Oguri, M., et al. 2007, *The Astronomical Journal*, 133, 2222
- Shen, Y., Brandt, W. N., Richards, G. T., et al. 2016, *The Astrophysical Journal*, 831, 7
- Shimasaku, K., Ouchi, M., Okamura, S., et al. 2003, *The Astrophysical Journal*, 586, 111
- Shimasaku, K., Hayashino, T., Matsuda, Y., et al. 2004, *The Astrophysical Journal*, 605, L93
- Shimasaku, K., Kashikawa, N., Doi, M., et al. 2006, *Publications of the Astronomical Society of Japan*, 5, 313
- Shioya, Y., Taniguchi, Y., Sasaki, S. S., et al. 2009, *The Astrophysical Journal*, 696, 546
- Simpson, C., Mortlock, D., Warren, S., et al. 2014, *Monthly Notices of the Royal Astronomical Society*, 442, 3454
- Sobacchi, E., & Mesinger, A. 2013a, *Monthly Notices of the Royal Astronomical Society*, 432, 3340
- . 2013b, *Monthly Notices of the Royal Astronomical Society: Letters*, 432, L51
- Susa, H., & Umemura, M. 2004, *The Astrophysical Journal*, 600, 1
- Swinbank, J., Baker, J., Barr, J., Hook, I., & Bland-Hawthorn, J. 2012, *Monthly Notices of the Royal Astronomical Society*, 422, 2980
- Thoul, A. A., & Weinberg, D. H. 1996, *The Astrophysical Journal*, 465, 608
- Toshikawa, J., Kashikawa, N., Ota, K., et al. 2012, *The Astrophysical Journal*, 750, 137
- Trainor, R. F., & Steidel, C. C. 2012, *The Astrophysical Journal*, 752, 39
- Trakhtenbrot, B., Lira, P., Netzer, H., et al. 2017, *The Astrophysical Journal*, 836, 8
- Trakhtenbrot, B., Netzer, H., Lira, P., & Shemmer, O. 2011, *The Astrophysical Journal*, 730, 7
- Trenti, M., & Stiavelli, M. 2008, *The Astrophysical Journal*, 676, 767
- Utsumi, Y., Goto, T., Kashikawa, N., et al. 2010, *The Astrophysical Journal*, 721, 1680
- van Dokkum, P. G. 2001, *Publications of the Astronomical Society of the Pacific*, 113, 1420
- Venemans, B. P., Röttgering, H. J. A., Miley, G. K., et al. 2007, *Astronomy & Astrophysics*, 461, 823
- Volonteri, M., & Rees, M. J. 2006, *The Astrophysical Journal*, 650, 669
- Weisz, D. R., Johnson, B. D., & Conroy, C. 2014, *The Astrophysical Journal*, 794, L3
- Wiersma, R. P. C., Schaye, J., & Smith, B. D. 2009, *Monthly Notices of the Royal Astronomical Society*, 393, 99
- Wu, X.-B., Wang, F., Fan, X., et al. 2015, *Nature*, 518, 512
- Wylezalek, D., Galametz, A., Stern, D., et al. 2013, *The Astrophysical Journal*, 769, 79
- Yoshida, M., Shimasaku, K., Kashikawa, N., et al. 2006, *The Astrophysical Journal*, 653, 988
- Zheng, W., Overzier, R. A., Bouwens, R. J., et al. 2006, *The Astrophysical Journal*, 640, 574
- Zheng, Z.-Y., Finkelstein, S. L., Finkelstein, K., et al. 2013, *Monthly Notices of the Royal Astronomical Society*, 431, 3589